Inorganic Chemistry

Article

pubs.acs.org/IC

$LnV_3Te_3O_{15}(OH)_3{\cdot}nH_2O$ (Ln = Ce, Pr, Nd, Sm, Eu, Gd; n = 1−2): A New Series of Semiconductors with Mixed-Valent Tellurium (IV,VI) Oxoanions

Jian Lin, Kariem Diefenbach, Jingcheng Fu, Justin N. Cross, Ronald J. Clark, and Thomas E. Albrecht-Schmitt*

Department of Chemistry and Biochemistry, Florida State University, 95 Chieftan Way, Tallahassee, Florida 32306, United States

Supporting Information

ABSTRACT: Six new lanthanide tellurium vanadates with the general formula $LnV_3Te_3O_{15}(OH)_3{\cdot}nH_2O$ (**LnVTeO**) (Ln = Ce, Pr, Nd, Sm, Eu, and Gd; n = 2 for Ce and Pr; n = 1 for Nd, Sm, Eu, and Gd) have been prepared hydrothermally via the reactions of lanthanide nitrates, TeO_2, and V_2O_5 at 230 °C. **LnVTeO** adopts a three-dimensional (3D) channel structure with a space group of $P6_3/mmc$. Surprisingly, two types of oxoanions: $Te^{IV}O_3^{2-}$ trigonal pyramids and $Te^{VI}O_6^{6-}$ octahedra, coexist in these compounds. Solid-state UV−vis−NIR absorption spectra for **LnVTeO** show approximate band gaps on the order of 1.9 eV, suggesting the wide band gap semiconducting nature of these materials. No magnetic phase transition was observed in any of the analogues, but a clear increase in the strength of short-range antiferromagnetic correlations was found with the shortening of distances between magnetically coupled Ln^{3+} ions in **LnVTeO**.

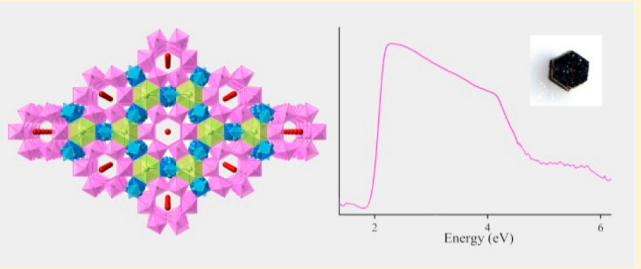

INTRODUCTION

The solid-state chemistry of tellurium oxoanion compounds is intricate owing to the diverse coordination geometries that Te^{IV} and Te^{VI} can adopt. In the former, Te^{IV} oxoanions (tellurite) possess a stereochemically active lone pair of electrons on the Te centers. Tellurite can be three-, four-, or even five-coordinate, forming trigonal pyramidal, disphenoidal, and square pyramidal geometries, respectively.[1] Secondary intermediate length Te···O contacts often further complicate unambiguous descriptions of the local geometries around Te^{IV}.[2] Tellurite can be further interconnected to form complex oligomeric and polymeric structures.[1c,3] While it might be expected that Te^{VI} oxoanion (tellurate) compounds would be much simpler, in fact, a series of complex equilibria connect the ostensibly octahedral TeO_6^{6-} anion with the tetrahedral TeO_4^{2-} anion.[3] The combination of tellurite and tellurate moieties in one compound is intriguing but difficult to achieve because Te^{VI} is easily reduced, and hence mixed-valent tellurium compounds are relatively rare. Examples of these atypical materials include Te_2O_5 ($Te^{IV}Te^{VI}O_5$), $SrTe^{IV}_2Te^{VI}O_8$, $Ag_2Te^{IV}_2Te^{VI}_2O_{11}$, $A_4V_6[Te_2^{IV}Te^{VI}]O_{24}$ (A = K, Rb), $Hg_2Te^{IV}Te^{VI}O_7$, and $Cs(M,Te)_2O_6$.[1b,4]

The distorted geometries of tellurium oxoanions lend themselves well to the creation of noncentrosymmetric materials. These structural features have been combined with second-order Jahn−Teller (SOJT) distorted d^0 early transition metals (e.g., Nb^{5+}, V^{5+}, and Mo^{6+}) to enhance properties associated with some types of acentricity (e.g., NLO, piezoelectricity, and pyroelectricity).[5] Examples of compounds in this class include $Ga_2MoTe_2O_{10}$,[6] $Ag_2Mo_3Te_3O_{16}$,[7] $Zn_2(MoO_4)(TeO_3)$,[8] $La(VO_2)_3(TeO_6){\cdot}3H_2O$,[9] $Cd_4V_2Te_3O_{15}$,[10] $Li(VO_2)_3(TeO_3)_2$,[11] $Cs(VO_2)_3(TeO_3)_2$,[12] and $Cs(VO_2)_3(SeO_3)_2$.[13] $La(VO_2)_3(TeO_6){\cdot}3H_2O$ is particularly relevant to the work reported herein because it combines the complexities associated with the high coordination numbers of lanthanides with the distortions common to high-oxidation state transition metals.[9] In addition, it is also a rare example of a Te^{VI} containing compound. One could envision expanding this further by incorporating an oxoanion containing Te^{IV} as well.

Our group has been interested for a number of years in preparing and characterizing lanthanide oxoanion systems that also incorporate early transition metals. This strategy, in fact, leads to acentric materials with pronounced NLO properties such as $LnMoO_2(IO_3)_4(OH)$ (Ln = Nd, Sm, Eu).[14] In addition, these sorts of complex materials are ideal for the fine-tuning of structure−property relationships as evidenced by the recent case of aliovalent substitution in the isotopic vanadate compounds, $Th(VO_3)_2(SeO_3)$ and $Ln(VO_3)_2(IO_3)$ (Ln = Ce, Pr, Nd, Sm, and Eu).[15]

In oxoanion compounds, lanthanides are typically bonded to eight or nine oxygen atoms, although coordination numbers of seven through 10 are well represented. Numerous coordination environments are known because these coordination geometries undergo a large variety of distortions from ideal symmetries.[16] The diversity of coordination environments of

Received: May 9, 2014
Published: August 21, 2014

   dx.doi.org/10.1021/ic501068e | Inorg. Chem. 2014, 53, 9058−9064

Table 1. Crystallographic Data for $LnV_3Te_3O_{15}(OH)_3{\cdot}nH_2O$ (LnVTeO) (Ln = Ce, Pr, Nd, Sm, Eu, and Gd; n = 2 for Ce and Pr; n = 1 for Nd, Sm, Eu, and Gd)

compound	Ce	Pr	Nd	Sm	Eu	Gd
formula mass	1002.74	1003.53	988.86	994.97	996.58	1001.87
color	dark red	dark red	dark red	dark red	dark red	dark red
habit	hexagonal	hexagonal	hexagonal	hexagonal	hexagonal	hexagonal
space group	$P6_3/mmc$	$P6_3/mmc$	$P6_3/mmc$	$P6_3/mmc$	$P6_3/mmc$	$P6_3/mmc$
a (Å)	12.166(5)	12.1147(9)	12.1075(14)	12.1068(6)	12.0731(9)	12.0745(13)
c (Å)	12.537(5)	12.4949(9)	12.4572(15)	12.4509(6)	12.3674(10)	12.3701(14)
V (Å^3)	1606.9(15)	1588.1(3)	1581.5(4)	1580.48(17)	1561.2(3)	1561.9(4)
Z	4	4	4	4	4	4
T (K)	100	100	100	100	100	100
λ (Å)	0.71073	0.71073	0.71073	0.71073	0.71073	0.71073
maximum 2θ (deg)	26.371	26.358	26.368	26.368	26.345	26.340
ρ_{calcd} (g cm^{-3})	4.116	4.168	4.132	4.161	4.219	4.239
μ (Mo Kα) (cm^{-1})	99.14	102.21	104.70	109.07	112.98	115.24
$R(F)$ for $F_o^2 > 2\sigma(F_o^2)^a$	0.0389	0.0396	0.0280	0.0261	0.0357	0.0228
$R_w(F_o^2)^b$	0.1017	0.1074	0.0899	0.0812	0.1028	0.0717

$^aR(F) = \Sigma||F_o| - |F_c||/\Sigma|F_o|$. $^bR_w(F_o^2) = [\Sigma[w(F_o^2 - F_c^2)^2]/\Sigma\, wF_o^4]^{1/2}$.

lanthanides enables vastly different manners of bonding with ligands. The incorporation of lanthanides into these compounds can provide both large magnetic moments and considerable single ion anisotropy.[17] The optical properties of lanthanide ions such as luminescence allow one to couple optical and magnetic properties.[18] Applying the aforementioned mixed-anions system to the study of lanthanide materials is a promising route of creating new solids with interesting physicochemical properties. In an attempt to prepare lanthanide-containing materials that allow for comparisons in bonding and physical properties, using tellurium-vanadate systems, $LnV_3Te_3O_{15}(OH)_3{\cdot}nH_2O$ (**LnVTeO**; Ln = Ce, Pr, Nd, Sm, Eu, and Gd; n = 2 for Ce and Pr; n = 1 for Nd, Sm, Eu, and Gd) were discovered. **LnVTeO** features a 3D channel structure constructed from lanthanide ions with mixed-valent tellurium (IV and VI) oxoanions and vanadate. In addition, **LnVTeO** appear to be wide band gap semiconductors.

EXPERIMENTAL SECTION

Synthesis. $Ce(NO_3)_3{\cdot}6H_2O$ (99.998%, Alfa-Aesar), $Pr(NO_3)_3$ (99.9%, Alfa-Aesar), $Nd(NO_3)_3{\cdot}6H_2O$ (99.9%, Alfa-Aesar), $Sm(NO_3)_3{\cdot}6H_2O$ (99.9%, Alfa-Aesar), $Eu(NO_3)_3{\cdot}6H_2O$ (99.9%, Alfa-Aesar), $Gd(NO_3)_3{\cdot}5H_2O$ (99.99%, Alfa-Aesar), V_2O_5 (99.6%, Alfa-Aesar), and TeO_2 (99.99%, Alfa-Aesar) were all used as received. Reactions were run in PTFE-lined Parr 4749 autoclaves with 23 mL internal volume autoclaves. Distilled and Millipore filtered water was used in all reactions.

$LnV_3Te_3O_{15}(OH)_3{\cdot}nH_2O$ (LnVTeO) (Ln = Ce, Pr, Nd, Sm, Eu, and Gd; n = 2 for Ce and Pr; n = 1 for Nd, Sm, Eu, and Gd). $Ln(NO_3)_3$ (0.5 mmol; 0.2171 g for $Ce(NO_3)_3{\cdot}6H_2O$, 0.1635 g for $Pr(NO_3)_3$, 0.2192 g for $Nd(NO_3)_3{\cdot}6H_2O$, 0.2222 g for $Sm(NO_3)_3{\cdot}6H_2O$, 0.2230 g for $Eu(NO_3)_3{\cdot}6H_2O$, 0.2167 g for $Gd(NO_3)_3{\cdot}5H_2O$), TeO_2 (1.5 mmol, 0.2394 g), V_2O_5 (1.5 mmol, 0.2728 g), and water (2 mL) were loaded into a 23 mL PTFE-lined autoclave liner. The autoclave was sealed and heated to 230 °C in a box furnace for 3 days. The autoclave was then cooled to room temperature at a rate of 5 °C/h. The products were washed with DI water to remove soluble solids, followed by rinsing with methanol. Dark red hexagonal crystals were isolated.

Crystallographic Studies. Single crystals of **LnVTeO** were mounted on CryoLoops with Krytox oil and optically aligned on a Bruker APEXII Quazar X-ray diffractometer using a digital camera. Initial intensity measurements were performed using an IμS X-ray source, a 30 W microfocused sealed tube (Mo Kα, λ = 0.71073 Å) with high-brilliance and high-performance focusing Quazar multilayer optics. Standard APEXII software was used for determination of the unit cells and data collection control. The intensities of reflections of a sphere were collected by a combination of four sets of exposures (frames). Each set had a different φ angle for the crystal, and each exposure covered a range of 0.5° in ω. A total of 1464 frames were collected with an exposure time per frame of 10 to 30 s, depending on the crystal. The SAINT software was used for data integration including Lorentz and polarization corrections. Semiempirical absorption corrections were applied using the program SADABS or TWINABS.[19] All five structures were solved by direct methods using SHELXT-2013 and refined by full-matrix least-squares fitting on F^2 by SHELXL-2013.[20] Selected crystallographic information is listed in Table 1. Atomic coordinates and additional structural information are provided in the Supporting Information (CIFs). All of the atoms were refined with anisotropic thermal parameters, and structures were checked for higher symmetry using PLATON.[21]

Single-crystal X-ray diffraction experiments on **LnVTeO** proved to be very challenging for many reasons. First, the crystals had a tendency to stack on one another. The crystals were also twinned in many cases. Second, it is difficult to determine the space group of the structure. One tellurium site and several oxygen atoms are disordered, leading one down the false path of trying to solve the structure in a noncentrosymmetric space group $P6_3mc$ (no. 186). The final solution of the structure was achieved using the latest program SHELXT, which solves relatively routine small molecule structures and determines the space group and structure together. All of these features are only compatible with the centrosymmetric space group $P6_3/mmc$ (no. 194), where a reasonable solution and refinement of the structure was finally achieved.

Scanning Electron Microscopy and Energy-Dispersive X-ray Spectrometry (SEM-EDS) Analysis. SEM-EDS images and data were collected using a LEO EVO 50 with an Oxford INCA energy-dispersive X-ray spectrometer. The energy of the electron beam was set at 29.02 kV, and the spectrum acquisition time was 120 s. All of the data were calibrated with standards, and all EDS results are provided in the Supporting Information.

UV−Vis Spectroscopy. UV−vis data were acquired from single crystals using a Craic Technologies microspectrophotometer. Crystals were placed on quartz slides under Krytox oil, and the data were collected from 200 to 900 nm. Using the absorbance data, absorbance versus optical energy plots were constructed to analyze the semiconductor nature of **LnVTeO**.

Thermogravimetric Analyses (TGA). TGA analyses were carried out with a TA Instruments Q600 unit, at a heating rate of 10 °C/min under a static argon atmosphere.

Magnetic Property Measurements. The magnetic susceptibilities of **LnVTeO** (Ln = Ce, Pr, Nd, and Sm) were measured on

dx.doi.org/10.1021/ic501068e | Inorg. Chem. 2014, 53, 9058−9064

polycrystalline samples using a superconducting quantum interference device (SQUID) magnetometer (Quantum Design MPMS-XL). **LnVTeO** (Ln = Eu, and Gd) are not included in this study owing to low yields and/or the presence of impurities. The DC magnetization was measured in an applied field of 0.1 T in the 1.8−300 K temperature range, and the field-dependent magnetization was evaluated at 1.8 K with the applied field varying from 0 to 5.5 T. The data were corrected for diamagnetic contributions using Pascal's constants.[22]

RESULTS AND DISCUSSION

Synthesis. All six compounds were synthesized using $Ln(NO_3)_3$, TeO_2, and V_2O_5 under hydrothermal conditions. The products consisted of dark red **LnVTeO** crystals (Figure 1) with 30−70% yields, coexisting in some cases with unreacted V_2O_5. The element components of **LnVTeO** were characterized by SEM-EDS, showing an approximate 1:3:3 molar ratio of Ln/Te/V in the compounds (cf. Figure S1). The key feature of this reaction is the use of lanthanide nitrates as opposed to using other lanthanide sources, e.g. lanthanide oxides and lanthanide chlorides, as they failed to generate **LnVTeO**. Under acidic conditions, the redox potential for Te^{IV}/Te^{VI} is 1.02 V/NHE.[23] The nitrate is necessary to oxidize Te^{IV} in the TeO_2 to Te^{VI} to produce **LnVTeO**.

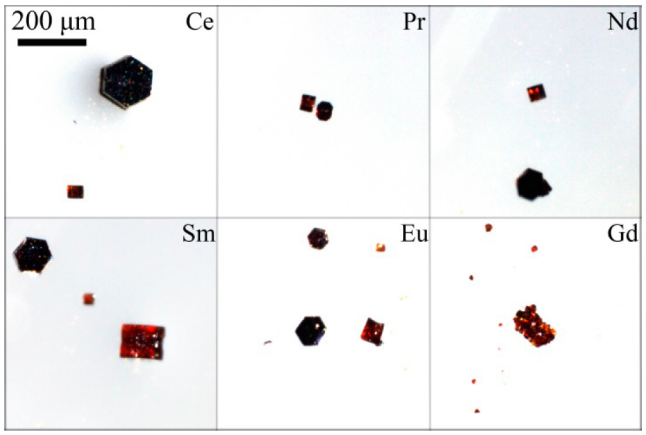

Figure 1. Crystal images of **LnVTeO**.

Structures and Topological Descriptions. Single crystal X-ray diffraction reveals that **LnVTeO** are isomorphous and crystallize in the space group $P6_3/mmc$. It is important to note that despite the fact that the building units (LnO_{10} and TeO_3) in these compounds lack inversion centers that the overall structure of **LnVTeO** is still centrosymmetric, and this illustrates that using distorted building units, even cooperatively, that have a high propensity for yielding acentric structures does not always yield a noncentrosymmetric framework. As shown in Figure 2a, the main features of the structure are the channels that extend down the *c* axis. In **CeVTeO** and **PrVTeO**, there is one crystallographically independent water molecule residing in the channels, but the water molecule in **CeVTeO** is disordered over two sites. In **NdVTeO**, **SmVTeO**, **EuVTeO**, and **GdVTeO**, X-ray diffraction studies reveal the presence of highly disordered entities within the channels. Unfortunately, the displacements of these entities with water molecules did not refine well. The 3D framework of **LnVTeO** can be divided into two components in order to be better understood, the Ln−Te−oxo moiety (Figure 2b) and six-membered vanadium rings (Figure 2d). The measured pore size of the Ln−Te−oxo moiety has a diameter of approximately 9.5 Å, which is large enough to house the vanadium rings.

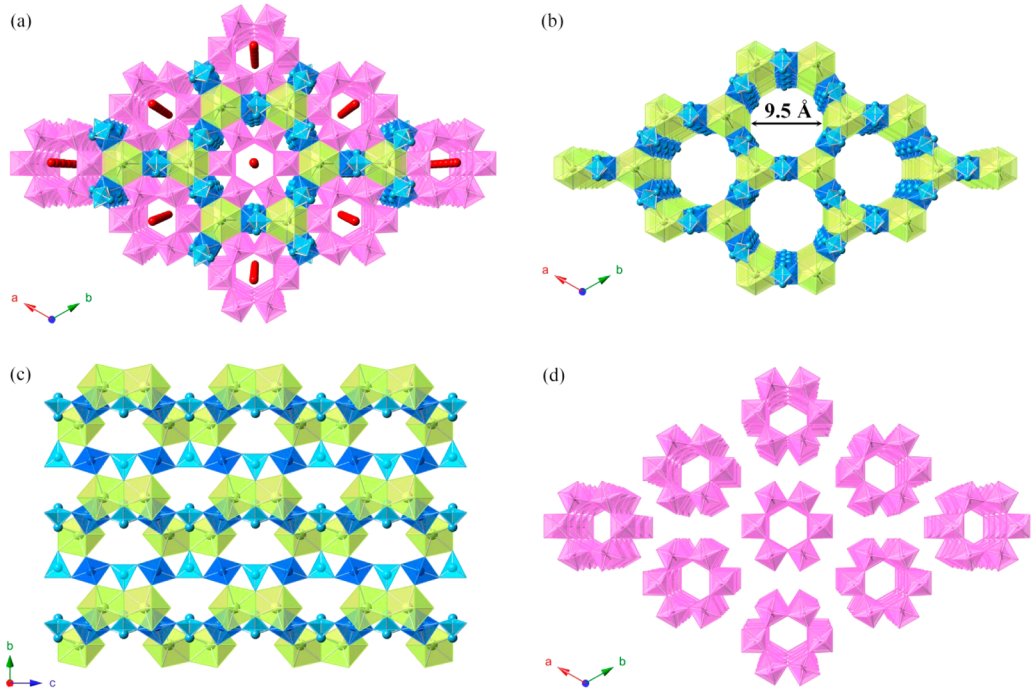

Figure 2. (a) A view of the 3D network structure of **LnVTeO** (Ln = Ce and Pr, the water molecules are highly disordered in the channels of Nd, Sm, Eu, and Gd). (b) A view of the Ln−Te−oxo moiety extending down the *c* axis. (c) A side view of Ln−Te−oxo moiety extending down the *a* axis. (d) A view of the six-membered vanadium rings. $Ln(1)O_{10}$ polyhedra are shown green, $Te(1)O_3$ in light blue, $Te(2)O_6$ in dark blue, and $V(1)O_6$ in purple, and the oxygen atoms are red spheres.

dx.doi.org/10.1021/ic501068e | Inorg. Chem. 2014, 53, 9058−9064

The Ln−Te−oxo moiety is constructed from one crystallographically unique Ln^{3+} ion bridged by two types of tellurium oxoanions with different valences: tellurite, which exists as TeO_3^{2-} trigonal pyramids, and tellurate, which exists as TeO_6^{6-} octahedra. A side view of Ln−Te−oxo moiety is available in Figure 2c. The Ln^{3+} ion resides on the 6_3 screw axis in the [001] direction and is coordinated by 10 O atoms, forming capped trigonal cupolas with C_{3v} symmetry (Figure 3a). Six

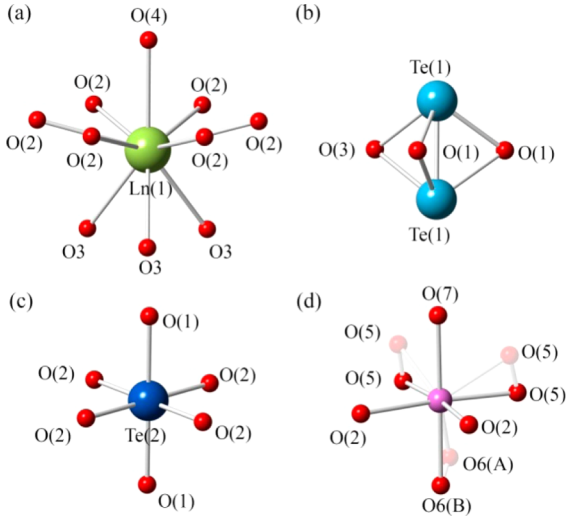

Figure 3. Coordination geometries of Ln, Te, and V in **LnVTeO**. $Ln(1)O_{10}$ polyhedra are shown green, $Te(1)O_3$ in light blue, $Te(2)O_6$ in dark blue, and $V(1)O_6$ in purple, and the oxygen atoms are red spheres.

symmetrically equivalent O(2) atoms are bound in the equatorial plane in a nearly coplanar manner and three O(3) atoms locate on the base plane. The RE−O bond distances decrease from Ce to the Gd analogue (cf. Table 2). This trend is consistent with the increasing localization and decreased shielding of the 4f orbitals given from the consequent ionic contraction. As previously stated, the Ln−Te−oxo moiety features two unique tellurium ions: Te(1) is tetravalent, and Te(2) is hexavalent, as shown in Figures 3b and c, respectively. The tetravalent Te ion adopts a trigonal pyramid geometry, bound with three O atoms, O(1), O(1), and O(3), with Te−O length ranging from 1.915(9) Å to 1.933(4) Å. Te(1) is disordered over two positions through a mirror plane with distances from 2.134(3) to 2.154(2) Å. The hexavalent Te ion is coordinated with six O atoms, O(1), O(1), O(2), O(2), O(2), and O(2), forming an approximately octahedral geometry. The Te(2)−O(2) bond lengths in the equatorial plane are relatively short, ranging from 1.902(5) Å to 1.912(4) Å. The axial Te(2)−O(1) bond lengths range from 1.925(7) Å to 1.946(7) Å. Bond valence sums (BVS) are calculated using measured bond distances and predetermined bond valence parameters to determine the valence state of the Te ions.[24] BVS for Te(1) and Te(2) were summarized in Table S1, indicating the tetravalent and hexavalent oxidation states of Te(1) and Te(2), respectively.

The channels of the Ln−Te−oxo moiety are occupied by six-membered vanadium rings that edge-share with the Ln^{3+} ions (Figure 2d). The vanadium ring is composed from a single crystallographically unique vanadate anion. The vanadate anions polymerize to form a V_6O_{30} cluster with 3-fold symmetry and an inversion center as shown in Figure S2. The crystallographically unique VO_6^{7-} anion has approximately octahedral geometry, which is common for a V(V)-containing system.[25] Within the VO_6^{7-} anion, three O atoms are disordered over two positions, respectively (Figure 3d). These disordered sites are approximately 50%/50% occupied for O(5)/O(5)′, O(5)′/O(5)″, and O(6A)/O(6B). The disordered O atoms result in relatively large standard deviation of the V−O bond lengths. The disordered O atoms make confident BVS assignments difficult. Averaged bond lengths of the disordered oxygen sites were used for the BVS calculation, indicating pentavalent oxidation states of V(1) (Table S1). The remaining positive charge needed to counterbalance the anionic framework is accomplished by protonating the O(4) on Ln(1) and O5(5), O(6) and O(7) on V(1), inferred from bond lengths and bond-valence considerations.

Spectroscopic Data. The absorption spectra of **LnVTeO** were obtained from thin crystals using a microspectrophotometer. The characteristic f−f transitions anticipated for these compounds are clearly resolved only in the Nd compound ($^4I_{9/2} \rightarrow {}^4S_{3/2}$ at 738 nm, $^4I_{9/2} \rightarrow {}^2H_{9/2}$ at 796 nm, and $^4I_{9/2} \rightarrow {}^4F_{3/2}$ at 828 nm) because large charge-transfer features from the vanadium units dominate the UV/visible regions of the spectra.[18c,26] The broad absorption from approximately 250 to 650 nm is probably indicative of wide band gap semiconducting behavior. However, it could also be a series of overlapping LMCT bands from the various oxo donors to V^V.

Using the absorbance data, absorbance versus optical energy plots were constructed to analyze the semiconductor nature of **LnVTeO**, as shown in Figure 4. All of the compounds show sharp decline in absorption around 2 eV. Plots of absorbance versus energy at the absorption edge (1.8 to 2.1 eV) show nearly linear dependence. Extrapolation of absorbance versus energy to absorbance = 0 provides an approximate band gap of 1.9 eV.[27]

Magnetic Properties. Temperature dependence of χ, χ^{-1} (inset), and χT for **LnVTeO** (Ln = Ce, Pr, Nd, and Sm) are shown in Figure 5. No signature of a magnetic phase transition was observed for any of the **LnVTeO** analogues down to 1.8 K based on susceptibilities (χ) vs temperature. Above 100 K for Nd and 50 K for the Ce, Pr, and Sm analogues, the inverse susceptibilities (χ^{-1}) obey the modified Curie−Weiss law, $1/\chi = 1/[\chi_{TIP} + C/(T - \theta)]$, where C, θ, and χ_{TIP} represent the Curie constant, the Weiss temperature, and the temperature independent paramagnetic (TIP) contribution, respectively. The negative Weiss temperatures indicate prevailing antiferromagnetic interactions between the nearest-neighbor Ln^{3+} ions. A systematic increase in the strength of antiferromagnetic exchange is observed as the nearest neighboring Ln^{3+}−Ln^{3+} distance decreases (Table 3) due to the lanthanide contraction, as indicated by pronouncedly more negative Weiss temperatures (−20(1) K for Ce^{3+}, −40(2) K for Pr^{3+}, and −50(3) K for Nd^{3+}, respectively). The effective magnetic moment was evaluated from the Curie constant, $C = N\mu_{eff}^2\mu_B^2/3k_B$, where N, μ_B, and k_B are Avogadro's number, Bohr magneton, and the Boltzmann constant, respectively.[28] The effective moment is equal to 2.40 μ_B for **CeVTeO**, 3.57 μ_B for **PrVTeO**, and 3.68 μ_B for **NdVTeO**, which is in good agreement with the theoretical value of 2.54 μ_B for Ce^{3+} ($^2F_{5/2}$, $J = 5/2$, $g = 6/7$), 3.58 μ_B for Pr^{3+} ($^3H_4$, $J = 4$, $g = 4/5$), and 3.62 μ_B for Nd^{3+} ($^4I_{9/2}$, $J = 9/2$, $g = 8/11$), respectively. The χT value decreases continually upon cooling. The occurrence of this behavior can be attributed to the splitting of the ground states by the crystal field.[29] The

dx.doi.org/10.1021/ic501068e | Inorg. Chem. 2014, 53, 9058−9064

Table 2. Selected Bond Distances (Å) for LnVTeO

compound	Ce	Pr	Nd	Sm	Eu	Gd
Ln(1)−O(2)	2.604(6)	2.595(5)	2.589(4)	2.584(4)	2.575(6)	2.573(4)
Ln(1)−O(2)′	2.604(6)	2.595(5)	2.589(4)	2.584(4)	2.575(6)	2.573(4)
Ln(1)−O(2)″	2.604(6)	2.595(5)	2.590(4)	2.584(4)	2.575(6)	2.573(4)
Ln(1)−O(2))‴	2.604(6)	2.595(5)	2.590(4)	2.584(4)	2.575(6)	2.573(4)
Ln(1)−O(2)⁗	2.604(6)	2.595(5)	2.590(4)	2.584(4)	2.575(6)	2.573(4)
Ln(1)−O(2)⁗′	2.604(6)	2.595(5)	2.590(4)	2.584(4)	2.575(6)	2.573(4)
Ln(1)−O(3)	2.535(8)	2.514(7)	2.497(6)	2.479(6)	2.460(7)	2.452(5)
Ln(1)−O(3)′	2.535(8)	2.514(7)	2.497(6)	2.479(6)	2.460(7)	2.452(5)
Ln(1)−O(3)″	2.535(8)	2.514(7)	2.497(6)	2.479(6)	2.460(7)	2.452(5)
Ln(1)−O(4)	2.54(1)	2.51(1)	2.51(1)	2.48(1)	2.45(1)	2.44(1)
Te(1)−Te(1)	2.142(3)	2.134(3)	2.144(2)	2.147(2)	2.144(3)	2.154(2)
Te(1)−O(1)	1.927(6)	1.924(6)	1.925(5)	1.927(5)	1.931(6)	1.933(4)
Te(1)−O(1)′	1.927(6)	1.924(6)	1.925(5)	1.927(5)	1.931(6)	1.933(4)
Te(1)−O(3)	1.918(10)	1.916(9)	1.924(7)	1.925(7)	1.915(9)	1.921(6)
Te(2)−O(1)	1.946(7)	1.932(7)	1.939(6)	1.942(5)	1.925(7)	1.937(5)
Te(2)−O(1)′	1.946(7)	1.932(7)	1.939(6)	1.942(5)	1.925(7)	1.937(5)
Te(2)−O(2)	1.909(5)	1.902(5)	1.905(4)	1.912(4)	1.908(5)	1.909(4)
Te(2)−O(2)′	1.909(5)	1.902(5)	1.905(4)	1.912(4)	1.908(5)	1.909(3)
Te(2)−O(2)″	1.909(5)	1.902(5)	1.905(4)	1.912(4)	1.908(5)	1.909(3)
Te(2)−O(2)‴	1.909(5)	1.902(5)	1.905(4)	1.912(4)	1.908(5)	1.909(3)
V(1)−O(2)	1.970(5)	1.957(5)	1.969(4)	1.971(4)	1.968(5)	1.970(4)
V(1)−O(2)′	1.970(5)	1.957(5)	1.969(4)	1.971(4)	1.968(5)	1.970(4)
V(1)−O(5)	1.81(1)	1.79(1)	1.79(1)	1.80(1)	1.79(1)	1.79(1)
V(1)−O(5)″	1.81(1)	1.79(1)	1.79(1)	1.80(1)	1.79(1)	1.79(1)
V(1)−O(5))‴	1.81(1)	1.81(1)	1.80(1)	1.78(1)	1.80(1)	1.79(1)
V(1)−O(5)⁗	1.81(1)	1.80(11)	1.80(1)	1.78(1)	1.80(1)	1.79(1)
V(1)−O(6A)	1.53(2)	1.54(2)	1.53(2)	1.52(3)	1.49(3)	1.52(2)
V(1)−O(6B)	1.93(2)	1.92(2)	1.90(2)	1.84(2)	1.86(3)	1.89(2)
V(1)−O(7)	1.94(2)	1.93(2)	1.98(2)	2.03(2)	2.01(3)	2.04(2)

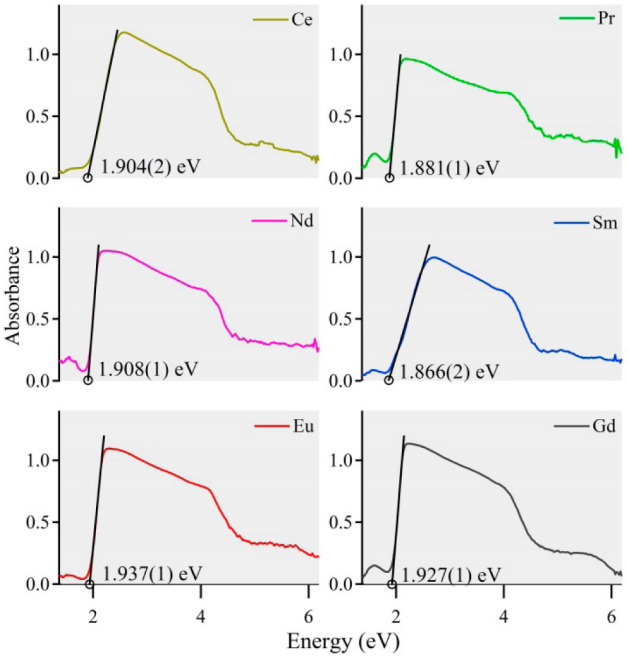

Figure 4. Optical energy spectrum of **LnVTeO** used to determine the approximate band gap. The least-squares fit is shown along with the x intercept that is the calculated band gap.

antiferromagnetic exchange is further supported by the suppressed magnetization values as compared to the Brillouin function for one Ln^{3+} ion at 1.8 K (Figure S3a,b,c).[30]

The Sm^{3+} ion is well-known to show Van Vleck paramagnetism due to the presence of low-lying excited states.[31] Consequently, the inverse susceptibility plot for **SmVTeO** exhibits strong deviation from the Curie−Weiss law (Figure 5d). As the sample is cooled down, the depopulation of excited states leads to the continuous decrease in χT that approaches zero at lower temperatures. The field-dependent magnetization measured at 1.8 K shows linear behavior with a relatively small maximum value of 0.21 μ_B for **SmVTeO** (Figures S4d). This finding suggests the Sm-containing compound is close to antiferromagnetic ordering that might occur at slightly lower temperatures than that available in our experiment.

CONCLUSIONS

In this study, a new series of lanthanide tellurium vanadates has been synthesized hydrothermally and characterized. The **LnVTeO** family represents a rare example of materials containing three different anions. The **LnVTeO** exemplifies another mixed-valent Te (IV and VI) oxo-anions containing materials. Single crystal X-ray diffraction reveals that **LnVTeO** crystallize in a high symmetry space group $P6_3/mmc$. Their structures exhibit a 3D framework consisting of Ln^{3+} ions, $Te^{IV}O_3^{2-}$ trigonal pyramids, $Te^{VI}O_6^{6-}$ octahedra, and $V^{V}O_6^{7-}$ octahedra. UV−vis absorption spectra for **LnVTeO** show band gaps at approximately 1.9 eV, suggesting the semiconducting nature of these compounds. Susceptibility studies suggest that no magnetic phase transitions occurs within the measured temperature ranges for any of the materials. Nevertheless, a clear increase in the strength of short-range antiferromagnetic correlations was observed with the decrease in the RE^{3+} ionic

dx.doi.org/10.1021/ic501068e | Inorg. Chem. 2014, 53, 9058−9064

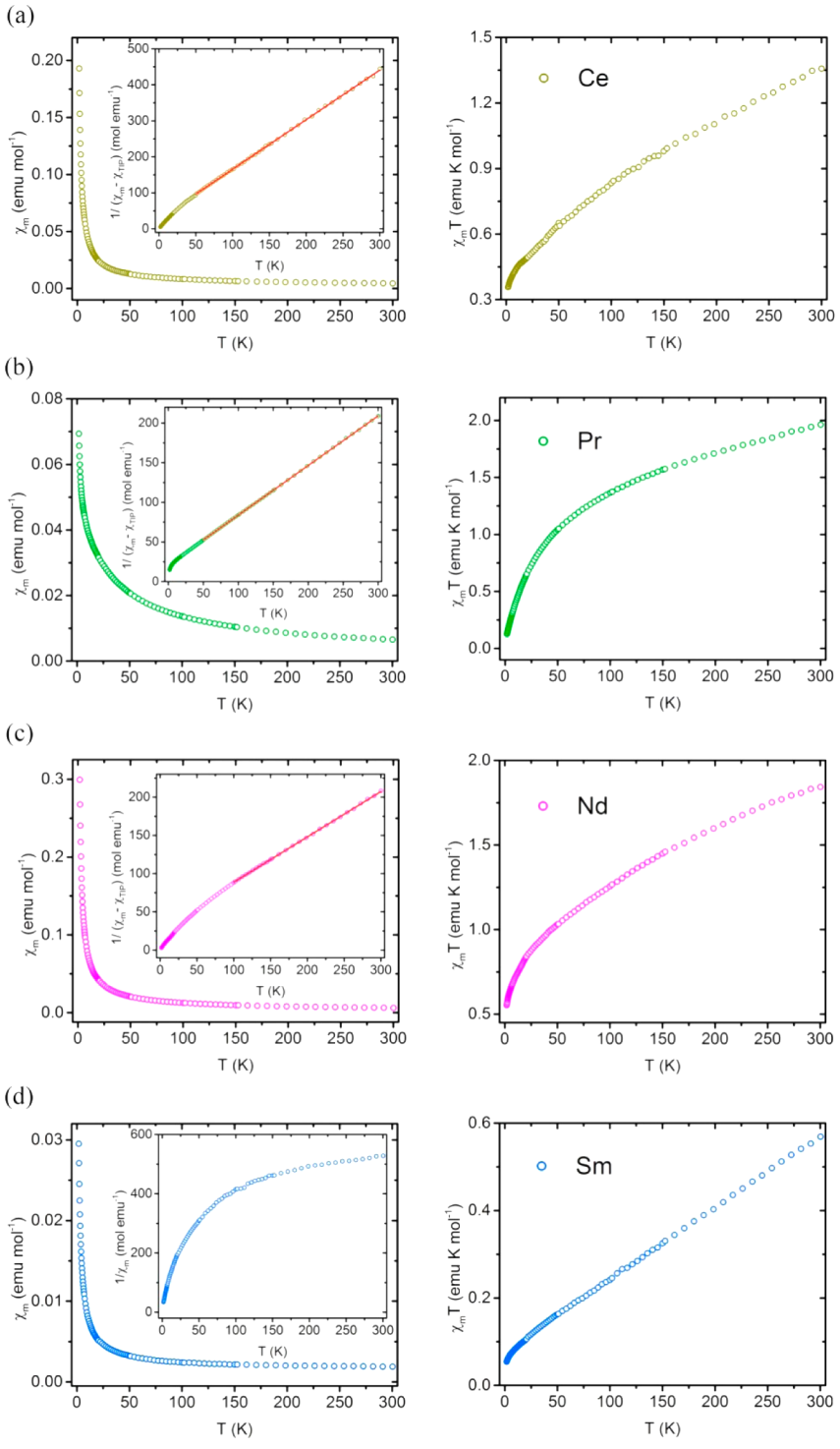

Figure 5. Temperature dependence of magnetic susceptibility χ, inverse susceptibility (inset), and the χT product for (a) **CeVTeO**, (b) **PrVTeO**, (c) **NdVTeO**, and (d) **SmVTeO**. The solid red line shows the theoretical fit to the modified Curie–Weiss law.

Table 3. Magnetic Data for LnVTeO

		Curie–Weiss Fitting			
				μ_{eff} (RE^{3+},μ_B)	
Ln	closest Ln–Ln (Å)	C (emu·K·mol^{-1})	θ (K)	from C	theo.
Ce	3.947(2)	0.72(1)	−20(1)	2.40	2.54
Pr	3.921(1)	1.59(1)	−40(2)	3.57	3.58
Nd	3.905(2)	1.69(4)	−50(3)	3.68	3.62

radius, consistent with the shortening of distances between magnetically coupled Ln^{3+} ions in **LnVTeO**. This study indicates that the Ln–d^0 containing complex with mixed anions could be an excellent system that allows for wide variations in composition and displayed electronic features. Investigations are underway to prepare analogues with additional transition metals and other lone-pair electron-containing anions.

dx.doi.org/10.1021/ic501068e | Inorg. Chem. 2014, 53, 9058–9064

■ ASSOCIATED CONTENT

Supporting Information

X-ray crystallographic files in CIF; SEM images and EDS spectra of **LnVTeO**; the field-dependent magnetization; TGA curves; and BVS values for Ln(1), Te(1), Te(2), and V(1) in **LnVTeO** are shown. This material is available free of charge via the Internet at http://pubs.acs.org.

■ AUTHOR INFORMATION

Corresponding Author

*E-mail: albrecht-schmitt@chem.fsu.edu.

Notes

The authors declare no competing financial interest.

■ ACKNOWLEDGMENTS

This material is based upon work supported by the U.S. Department of Energy, Office of Science, Office of Basic Energy Sciences, Heavy Elements Chemistry Program, under Award Number DE-FG02-13ER16414. This work was aslso supported by a Chinese Scholarship Council Graduate Fellowship to J.L.

■ REFERENCES

(1) (a) Jiang, H.-L.; Mao, J.-G. *Inorg. Chem.* **2005**, *45*, 717−721. (b) Zhu, T.; Qin, J.; Halasyamani, P. S. *Dalton Trans.* **2011**, *40*, 8527−8532. (c) Johnston, M. G.; Harrison, W. T. A. *J. Am. Chem. Soc.* **2002**, *124*, 4576−4577. (d) Irvine, J. T. S.; Johnston, M. G.; Harrison, W. T. A. *Dalton Trans.* **2003**, 2641−2645.

(2) Johnston, M. G.; Harrison, W. T. A. *Acta Crystallogr., Sect. E: Struct. Rep. Online* **2002**, *58*, i59−i61.

(3) Mao, J.-G.; Jiang, H.-L.; Kong, F. *Inorg. Chem.* **2008**, *47*, 8498−8510.

(4) (a) Lindqvist, O.; Moret, J. *Acta Crystallogr., Sect. B* **1973**, *29*, 643−650. (b) Barrier, N.; Malo, S.; Hernandez, O.; Hervieu, M.; Raveau, B. *J. Solid State Chem.* **2006**, *179*, 3484−3488. (c) Klein, W.; Curda, J.; Peters, E.-M.; Jansen, M. *Z. Anorg. Allg. Chem.* **2005**, *631*, 2893−2899. (d) Weil, M. *Z. Kristallogr.* **2003**, *218*, 691−698. (e) Siritanon, T.; Laurita, G.; Macaluso, R. T.; Millican, J. N.; Sleight, A. W.; Subramanian, M. A. *Chem. Mater.* **2009**, *21*, 5572−5574.

(5) Goodey, J.; Broussard, J.; Halasyamani, P. S. *Chem. Mater.* **2002**, *14*, 3174−3180.

(6) Kong, F.; Hu, C.-L.; Hu, T.; Zhou, Y.; Mao, J.-G. *Dalton Trans.* **2009**, 4962−4970.

(7) Zhou, Y.; Hu, C.-L.; Hu, T.; Kong, F.; Mao, J.-G. *Dalton Trans.* **2009**, 5747−5754.

(8) Nguyen, S. D.; Kim, S.-H.; Halasyamani, P. S. *Inorg. Chem.* **2011**, *50*, 5215−5222.

(9) Sivakumar, T.; Ok, K. M.; Halasyamani, P. S. *Inorg. Chem.* **2006**, *45*, 3602−3605.

(10) Jiang, H.-L.; Huang, S.-P.; Fan, Y.; Mao, J.-G.; Cheng, W.-D. *Chem.—Eur. J.* **2008**, *14*, 1972−1981.

(11) Johnston, M. G.; Harrison, W. T. A. *Acta Crystallogr., Sect. C: Cryst. Struct. Commun.* **2007**, *63*, i57−i59.

(12) Harrison, W. T. A.; Buttery, J. H. N. *Z. Anorg. Allg. Chem.* **2000**, *626*, 867−870.

(13) Harrison, W. T. A. *Acta Crystallogr., Sect. C: Cryst. Struct. Commun.* **2000**, *C56*, E422.

(14) Shehee, T. C.; Sykora, R. E.; Ok, K. M.; Halasyamani, P. S.; Albrecht-Schmitt, T. E. *Inorg. Chem.* **2002**, *42*, 457−462.

(15) Eaton, T.; Lin, J.; Cross, J. N.; Stritzinger, J. T.; Albrecht-Schmitt, T. E. *Chem. Commun.* **2014**, *50*, 3668−3670.

(16) (a) Lin, J.; Cross, J. N.; Diwu, J.; Polinski, M. J.; Villa, E. M.; Albrecht-Schmitt, T. E. *Inorg. Chem.* **2012**, *51*, 11949−11954. (b) Zehnder, R. A.; Wilson, C. S.; Christy, H. T.; Harris, K. S.; Chauhan, V.; Schutz, V.; Sullivan, M.; Zeller, M.; Fronczek, F. R.; Myers, J. A.; Dammann, K.; Duck, J.; Smith, P. M.; Okuma, A.; Johnson, K.; Sovesky, R.; Stroudt, C.; Renn, R. A. *Inorg. Chem.* **2011**, *50*, 836−846. (c) Lin, J.; Diwu, J.; Cross, J. N.; Villa, E. M.; Albrecht-Schmitt, T. E. *Inorg. Chem.* **2012**, *51*, 10083−10085. (d) Wang, C.-M.; Wu, Y.-Y.; Hou, C.-H.; Chen, C.-C.; Lii, K.-H. *Inorg. Chem.* **2009**, *48*, 1519−1523. (e) Baggio, R.; Garland, M. T.; Moreno, Y.; Pena, O.; Perec, M.; Spodine, E. *J. Chem. Soc., Dalton Trans.* **2000**, 2061−2066. (f) Polinski, M. J.; Alekseev, E. V.; Darling, V. R.; Cross, J. N.; Depmeier, W.; Albrecht-Schmitt, T. E. *Inorg. Chem.* **2013**, *52*, 1965−1975.

(17) Sorace, L.; Benelli, C.; Gatteschi, D. *Chem. Soc. Rev.* **2011**, *40*, 3092−3104.

(18) (a) Bünzli, J.-C. G.; Eliseeva, S. V. *Chem. Sci.* **2013**, *4*, 1939−1949. (b) Bünzli, J.-C. G. *Chem. Rev.* **2010**, *110*, 2729−2755. (c) Binnemans, K.; Görller-Walrand, C. *Chem. Phys. Lett.* **1995**, *235*, 163−174. (d) Lin, J.; Diefenbach, K.; Cross, J. N.; Babo, J.-M.; Albrecht-Schmitt, T. E. *Inorg. Chem.* **2013**, *52* (22), 13278−13281. (e) Lin, J.; Chai, P.; Diefenbach, K.; Shatruk, M.; Albrecht-Schmitt, T. E. *Chem. Mater.* **2014**, *26*, 2187−2194.

(19) (a) *SADABS*; *TWINABS*; Bruker: Madison, WI, 2001. (b) *SAINT*; Bruker: Madison, WI, 2007.

(20) Sheldrick, G. *Acta Crystallogr., Sect. A* **2008**, *64*, 112−122.

(21) Spek, A. L. *J. Appl. Crystallogr.* **2003**, *36*, 7−13.

(22) Bain, G. A.; Berry, J. F. *J. Chem. Educ.* **2008**, *85*, 532.

(23) (a) Bard, A. J.; Parsons, R.; Jordan, J. *Standard Potentials in Aqueous Solution*; Taylor & Francis: Oxfordshire, U. K., 1985. (b) Bouroushian, M. *Electrochemistry of Metal Chalcogenides*; Springer: New York, 2010.

(24) Brese, N. E.; O'Keeffe, M. *Acta Crystallogr., Sect. B* **1991**, *47*, 192−197.

(25) (a) Yang, Y. L.; Qiu, L.; Harrison, W. T. A.; Christoffersen, R.; Jacobson, A. J. *J. Mater. Chem.* **1997**, *7*, 243−248. (b) Harrison, W. T. A.; Dussack, L. L.; Jacobson, A. J. *Inorg. Chem.* **1996**, *35*, 1461−1467.

(26) (a) Carnall, W. T.; Fields, P. R.; Rajnak, K. *J. Chem. Phys.* **1968**, *49*, 4424−4442. (b) Carnall, W. T.; Fields, P. R.; Rajnak, K. *J. Chem. Phys.* **1968**, *49*, 4412−4423. (c) Carnall, W. T.; Fields, P. R.; Rajnak, K. *J. Chem. Phys.* **1968**, *49*, 4447−4449. (d) Carnall, W. T.; Fields, P. R.; Rajnak, K. *J. Chem. Phys.* **1968**, *49*, 4450−4455.

(27) Pankove, J. I. *Optical Processes in Semiconductors*; Dover: Mineola, NY, 1971.

(28) Carlin, R. L. *Magnetochemistry*; Springer-Verlag: Berlin, 1986.

(29) (a) Andruh, M.; Bakalbassis, E.; Kahn, O.; Trombe, J. C.; Porcher, P. *Inorg. Chem.* **1993**, *32*, 1616−1622. (b) Kahn, M. L.; Sutter, J.-P.; Golhen, S.; Guionneau, P.; Ouahab, L.; Kahn, O.; Chasseau, D. *J. Am. Chem. Soc.* **2000**, *122*, 3413−3421.

(30) Li, P.-X.; Zhang, S.-Y.; Mao, J.-G. *Dalton Trans.* **2010**, *39*, 11560−11567.

(31) Buschow, K. H. J.; De Boer, F. R. *Physics of Magnetism and Magnetic Materials*; Springer: London, 2012.